



4<sup>th</sup> IASPEI / IAEE International Symposium:

## Effects of Surface Geology on Seismic Motion

August 23–26, 2011 • University of California Santa Barbara

### Estimation of local site effects in the Upper Valais (Switzerland)

**Jan Burjánek**

ETH Zürich  
Sonneggstrasse 5  
8092 Zürich  
Switzerland

**Gabriela Gassner-Stamm**

ETH Zürich  
Sonneggstrasse 5  
8092 Zürich  
Switzerland

**Valerio Poggi**

ETH Zürich  
Sonneggstrasse 5  
8092 Zürich  
Switzerland

**Donat Fäh**

ETH Zürich  
Sonneggstrasse 5  
8092 Zürich  
Switzerland

#### ABSTRACT

The Valais is the area of greatest seismic hazard in Switzerland and has experienced a magnitude 6 or larger event every 100 years. Due to river regulations and engineering progress in the last two centuries, seismically unfavorable sites have become attractive for expanded settlement and industries. We present a result of extensive ambient noise measurement campaigns performed recently in the Visp - Matter valley area. The aim of these measurements is the development of the detailed 3D velocity model of the area for the realistic strong ground motion synthesis. However, as the extent of the dataset allows for systematic comparisons of the methods, the results can have a general impact. Particularly, the array measurements were processed by means of three-component high-resolution f-k method estimating both Love and Rayleigh dispersion curves. The ellipticity of Rayleigh waves was estimated by both new array-based and wavelet-based techniques for all array measurements. Locally 1D velocity profiles were obtained by joint inversions of the dispersion curves and the Rayleigh wave ellipticities. Finally, a temporary seismic network was deployed in the area to record weak ground motion due to local and regional earthquakes. Site-to-reference spectral ratios were calculated for the recorded events and compared with H/V curves obtained from ambient noise.

#### INTRODUCTION

The region of Canton Valais has the highest seismic hazard in Switzerland, experiencing a magnitude 6 or larger earthquake roughly every 100 years (1524, 1584, 1685, 1755, 1855, 1946). Due to river regulations and engineering progress in the last two centuries, seismically unfavorable sites have become attractive for expanded settlement and industries (Fig. 1), so the *seismic risk* increased considerably. In particular, the area near Visp holds special interest, as damaging earthquakes occur on average every 40 years (Intensity VI-VIII) with the most recent in 1960 reaching a macroseismic intensity of VII (Fäh *et al.*, 2011). The Visp event of 1855 ( $M_w \sim 6.2$ ) was the largest in Switzerland during the last 300 years. All such events were associated with significant damage resulting from strong ground motion and different kinds of secondary phenomena, including liquefaction in the Rhone plain (Fritsche *et al.*, 2006). As there are no available instrumental observations of these phenomena for the region, numerical modeling is the best method to improve predictions for future events. Thus, the main goal is to develop a detailed 3D velocity model of the area for realistic strong ground motion simulation. In this paper, we present a result of extensive ambient noise measurement campaign, the analysis of weak motion recordings obtained by local seismic network, and the development of the 3D velocity model.

#### INSTALLATION OF SEMI-PERMANENT SEISMIC ARRAY AND DATA ANALYSIS

Temporary seismic network was deployed in the Visp area during both winters 07/08 and 08/09. The aim of this temporary network was mainly to record weak ground motion due to local and regional earthquakes. The weak motion recordings are especially useful for an estimation of the relative site effects. Particularly, site-to-reference spectral ratios are useful for linear site response estimation (Borcherdt, 1970). Moreover, such semi-permanent array could serve generally as a source of information on 2D/3D seismic wave propagation effects in the area – detection of the refracted surface waves from the basin edges, estimation of the depth of the bedrock from converted phases, direct estimation of Green's functions between the stations using noise correlation techniques.

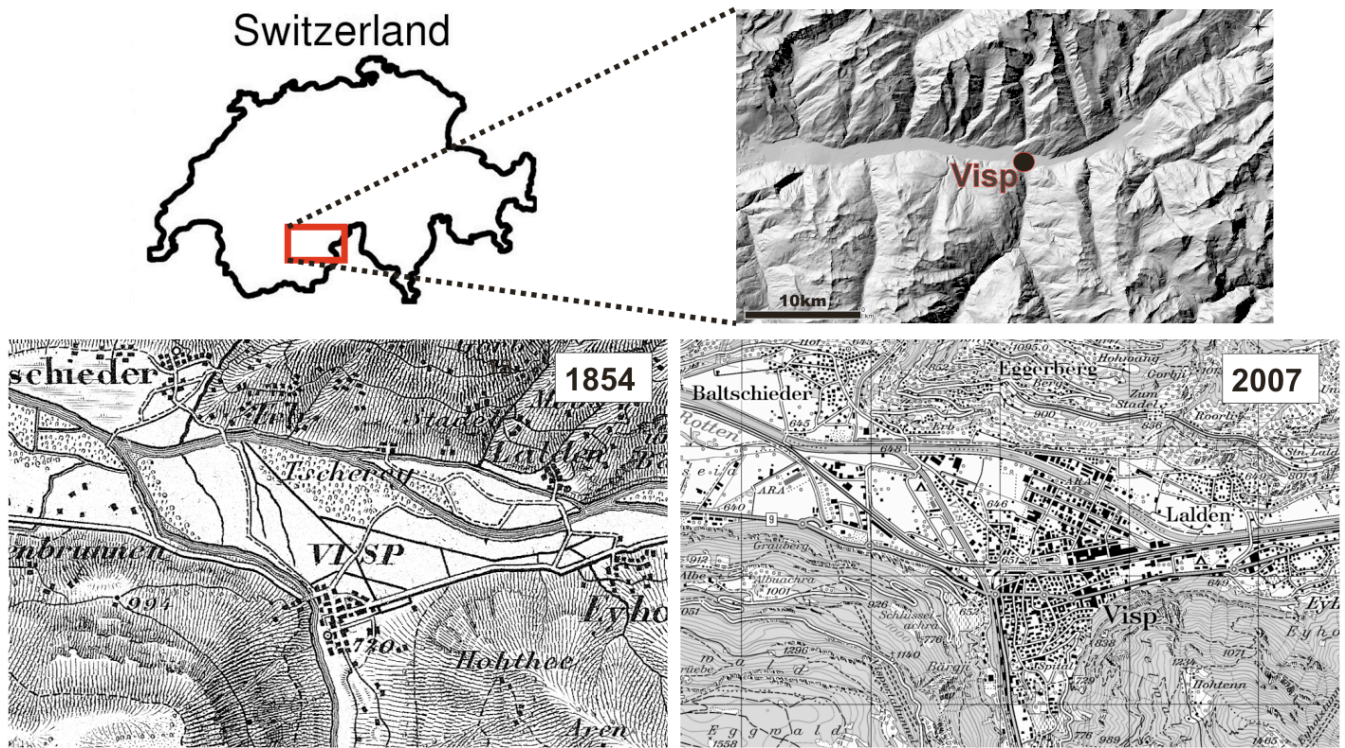


Fig. 1. Location of Visp within the Rhone valley (relief map at top), and the development of the Visp area in last 150 years.

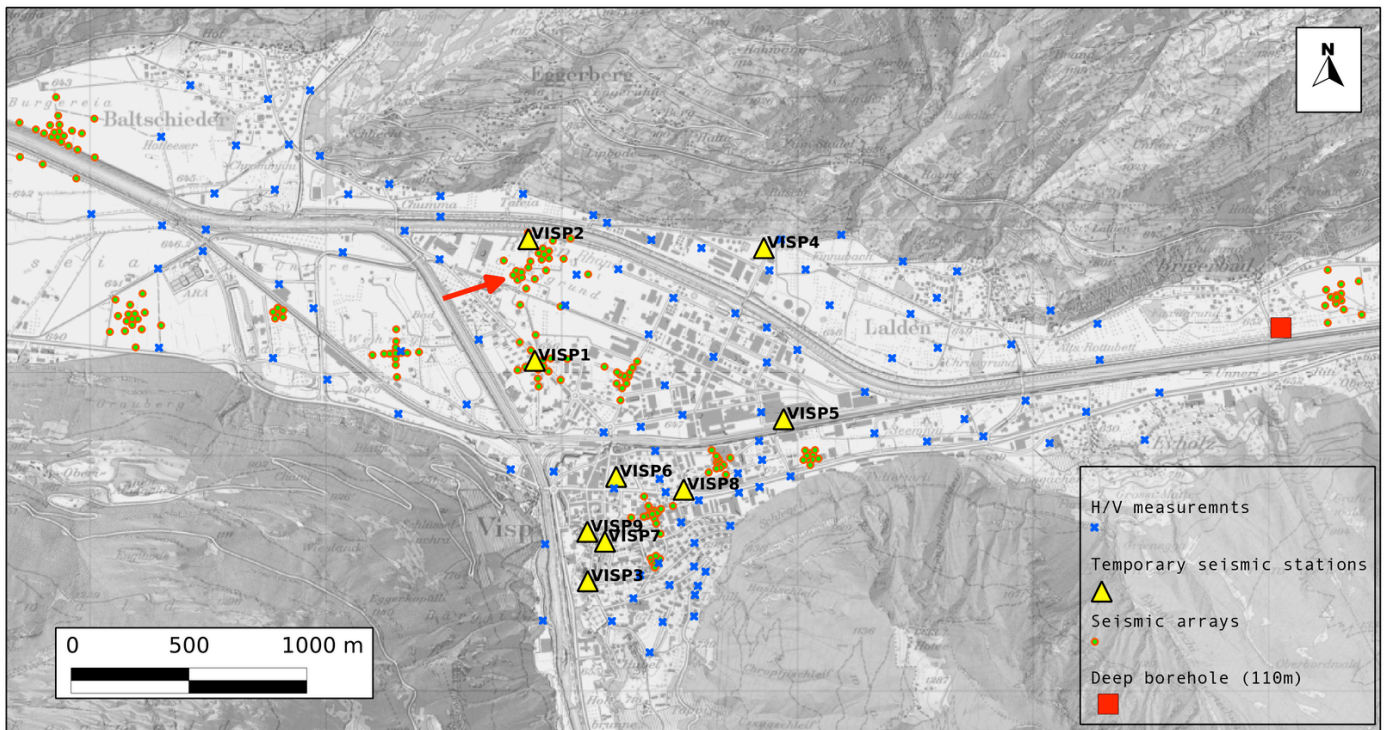


Fig. 2. Overview of measurements performed in the Visp area. Ambient noise array measurements are shown as green dots, single-station measurements as blue crosses, temporary stations as yellow triangles. Red square indicates the location of only deeper borehole (~110 m) in the area. Red arrow points at the location of planned borehole site (five boreholes 15-150 m), which will be instrumented by several seismic, deformation and pore-pressure sensors.

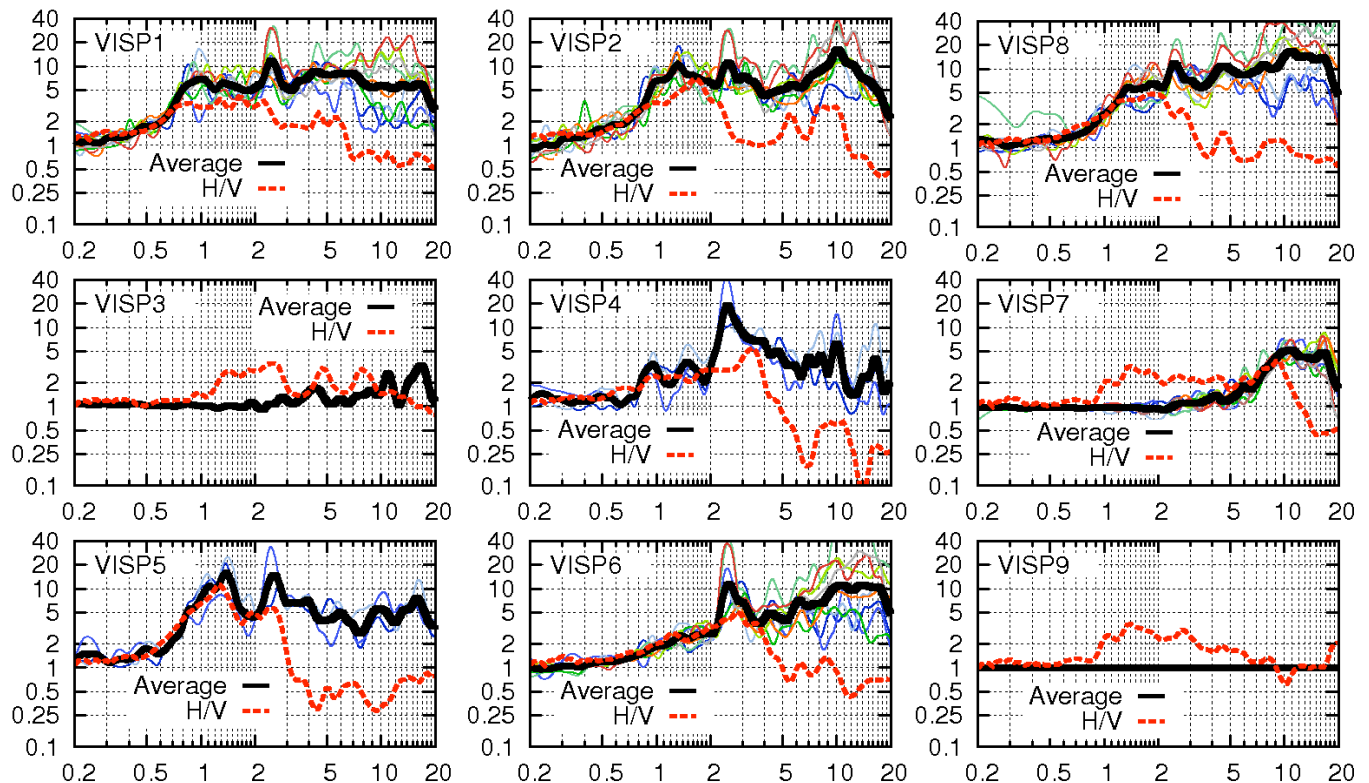


Fig. 3. Comparison of the mean site-to-reference spectral ratios (black thick) for earthquake recordings with H/V curves (dashed red) from ambient noise for the Visp area. VISP9 was the reference station. Colors distinguish between different events. A peak at 2.5 Hz has likely an industrial origin.

Eight temporary seismic stations were installed in Visp from November 2007 to Mai 2008 (VISP1-8, see Fig. 2). All stations consisted of Quanterra Q330 digitizer and LE3D-5s short period (SP) sensor. Four of the stations were additionally equipped with a broadband (BB) STS-2 sensor. The aim of the collocation of the BB and SP sensors was to extend the frequency band of the recordings for the future application of the noise correlation technique. Stations were setup to record continuous data with a sampling rate of 200 Hz. Further, seven temporary seismic stations were installed in Visp from November 2008 to April 2009 (VISP1-2, VISP5-9, see Fig. 2). Station VISP3 was replaced by station VISP9, since it was not possible to install VISP3 again during winter 08/09. VISP4 was located within the industrial facility of the Lonza factory. As it was an extremely noisy site, it was not setup up again during winter 08/09. Stations VISP1, VISP2, VISP4, VISP5 were located on the Rhone plain, where the strong site effects are expected due to sedimentary basin (Fritsche *et al.*, 2006). VISP6, VISP7, VISP8 were located close to the possible basin edge. Finally VISP3 and VISP9 were located on the rock outcrop and should serve as reference stations. Further information can be found in Burjanek *et al.* (2010a).

## Method

Regional seismic events were identified on the recordings with the help of the Swiss earthquake catalog. Site-to-reference spectral ratios were calculated following Borchardt (1970), under the assumption that the sources of the events are far from the array (especially compared to reference-to-site distances) and omitting source radiation, directivity and path effects. A window containing the intense S-wave part of the seismograms was selected manually for each recording and the Fourier transform was performed. The amplitude spectra were smoothed using the window proposed by Konno and Ohmachi (1998) with a bandwidth of 40 samples ( $b=40$ ). Finally, the total spectral amplitude in the horizontal direction was computed and divided by the Fourier amplitude of the reference station.

## Results

Three significant events were identified in the recordings from winter 07/08 and nine events in the recordings from winter 08/09. The seismograms are very noisy. The main source of the noise was located in the Lonza factory, probably close to the station VISP4. The frequency content of this industrial noise is localized around 2.5 Hz, 4 – 5 Hz and 9 – 10 Hz. Some of the stations placed in the

transformer houses are affected by noise at frequencies close to 50 Hz (e.g., VISP7). Resulting site-to-reference spectral ratios (SRSR) are plotted in Fig. 3. An average H/V curve retrieved from ambient noise by classical method is also plotted for each site.

Station VISP9 was selected as the main reference station. VISP9 was not operating during winter 07/08, VISP3 was the reference for that time period. VISP7 was selected for an estimation of the average VISP3/VISP9 ratio since it provided most stable results with well-defined mean among the stations operating during both winters. Spectral ratios from winter 07/08 were afterwards corrected for the average VISP3/VISP9 ratio to get the ratios with respect to VISP9. Note that VISP3 has a slightly different response from VISP9. Although the signal-to-noise ratio is low, the SRSR are quite stable below 5 Hz for all sites. The peak at 2.5 Hz, which is present on almost all sites, has the origin in the industrial noise, so the SRSRs do not represent the relative amplification close to this frequency. As the signal-to-noise ratio was systematically very low for the station VISP4, SRR for frequencies higher than 2 Hz cannot be considered at all for this station. Average SRSRs are in good agreement with H/V curves below the fundamental frequencies of the sites. H/V ratios do not agree with spectral ratios at VISP3 and VISP7 for frequencies between 1 to 5 Hz. This can be partially explained by industrial noise peaks (at 2.5, 4.5, 9 Hz) and radiation from the basin (1 Hz). Both of these effects should be suppressed in the site-to-reference spectral ratios

## AMBIENT NOISE MEASUREMENT CAMPAIGN

An extensive ambient noise measurement campaign was performed in the area (13 small-aperture arrays, almost 150 single-station measurements; see Fig. 2). The aim of the array measurements was to constrain the average shear-wave velocity of the main geological layers, identify the key interfaces, and map the lateral velocity variations. Single-station measurements were used to map changes in the interface depth between the layers. Array measurements were processed by means of a three-component, high-resolution f-k method estimating both Love and Rayleigh dispersion curves (Fäh *et al.*, 2008). The ellipticity of Rayleigh waves was estimated for all array measurements by both new array-based (Poggi and Fäh, 2009) and wavelet-based techniques (Fäh *et al.*, 2009). Locally 1D velocity profiles were finally obtained by joint inversion of the dispersion curves and Rayleigh wave ellipticities.

Let us briefly describe the new methods of the Rayleigh wave ellipticity estimation. The array method (f-k method) is based on the assumption that a peak in the f-k cross-spectrum obtained from horizontal (radial-polarized) and vertical components of motion must be representative of the signal power of a particular Rayleigh wave mode. Thus the relative frequency-dependent surface displacement ratio can be calculated for each mode separately, once the mode-correspondent dispersion curve is identified on the f-k plane.

In the wavelet-based method of the ellipticity estimation, the time-frequency representations of the vertical and both horizontal components are computed using continuous wavelet transform (CWT). In contrast to Love waves, Rayleigh waves will have an energy maximum on the vertical component. Therefore, to extract mostly Rayleigh waves, the absolute value of the CWT for the vertical component is scanned for all maxima. For each maximum identified on the time axis, the value of horizontal component wavelet coefficient is picked with a delay of one quarter of period. That is the theoretical delay between vertical and horizontal components for a Rayleigh wave. It can be positive (prograde particle motion) or negative (retrograde particle motion). The ratio between horizontal and vertical values is saved for each maximum found on the vertical component. Ratios are analyzed statistically, and the whole process is repeated for all frequencies, so the ellipticity of fundamental Rayleigh wave is estimated.

### Array measurements

Complete results of the measurement survey can be found in Burjanek *et al.* (2010b). Here we present the result for the *Brigerbad* array, which was located close to a deep borehole west of Visp (Fig. 2). Recordings were processed by two different codes (GEOPSY – Wathelet *et al.*, 2008; and three-component f-k method – Poggi and Fäh, 2009). All picked dispersion curves for both Love and Rayleigh waves are plotted in Fig. 4a. Note the remarkable agreement between two codes for the vertical component. It was possible to follow the dispersion curve of fundamental mode of both Rayleigh and Love wave down to 1.5 Hz. It was also possible to pick higher modes, particularly the first higher mode of Rayleigh wave. A complex behavior of the points picked in f-k plane for the horizontal components requires a careful interpretation. The dispersion curve picked for the radial component is interpreted in following way: below 3 Hz picked points follow the Love fundamental mode, between 3 and 5 Hz follow the Rayleigh fundamental mode, between 5 and 15 Hz follow the Rayleigh first higher mode, and for higher frequencies oscillate again between the Rayleigh and Love fundamental modes, respectively. A ghost of Rayleigh first higher mode can be observed on the transversal component. Rayleigh wave ellipticity was estimated for each array by both f-k and wavelet-based methods. All ellipticity curves are depicted in Fig. 4b. Ellipticity curves are in good agreement across the array in the frequency range of 1-20 Hz. The peak at 2.5 Hz is artificial and probably related to some continuously operating machine in the Lonza factory.

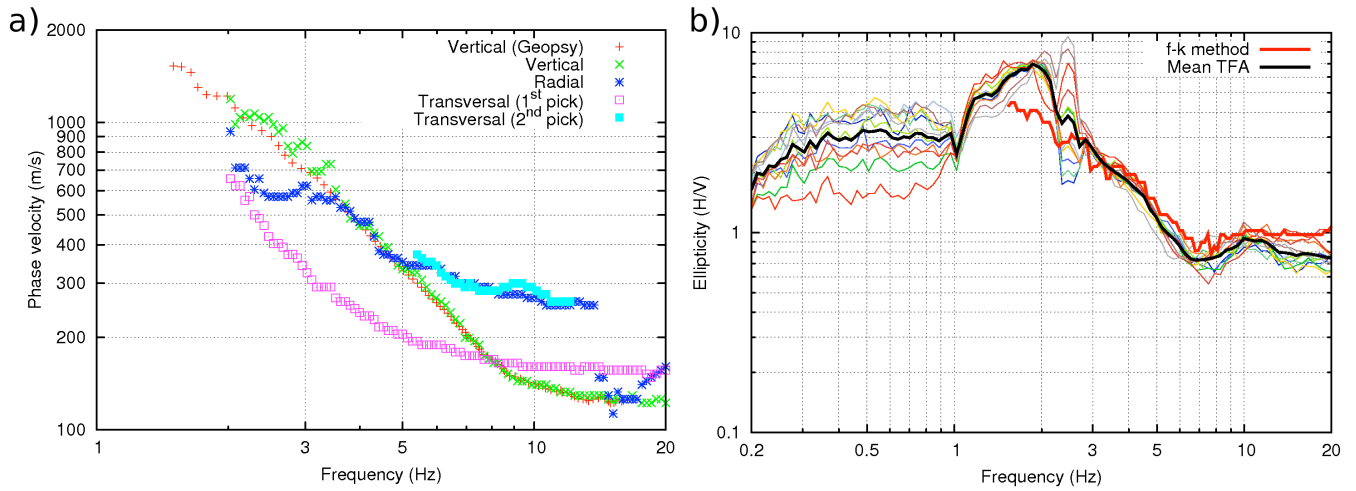


Fig. 4. Picked dispersion curves for Brigerbad array (a): fundamental mode of Rayleigh waves picked for vertical component (red, green), fundamental mode of Love waves (magenta) picked for transversal component, higher mode of Rayleigh waves picked for radial component (blue) and ghost of Rayleigh higher mode picked for transversal component (cyan). Rayleigh wave ellipticity curves for Brigerbad array (b): obtained by wavelet method - TFA (thin solid curves, black bold curve is a mean curve) and f-k method (bold red curve).

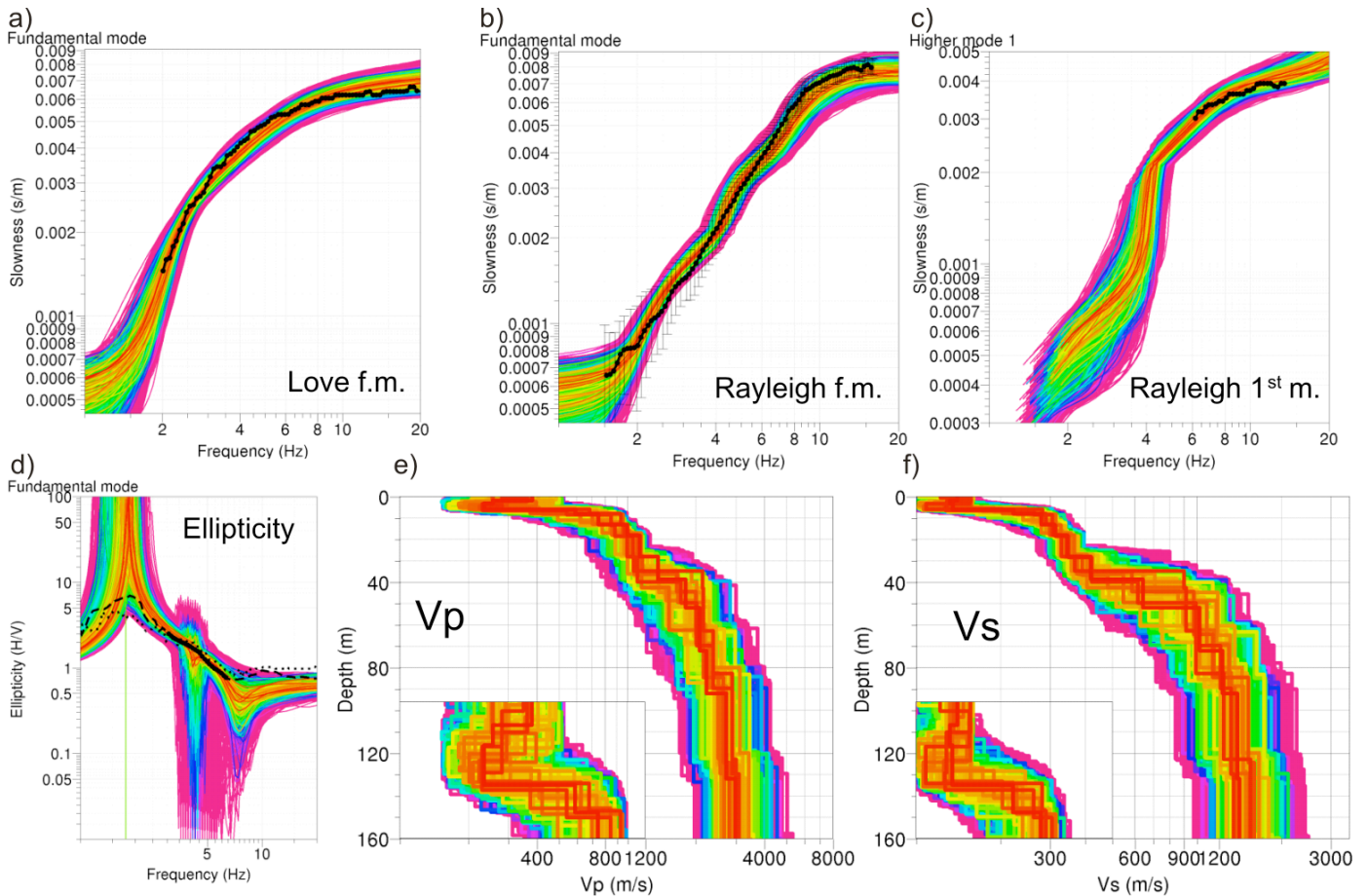


Fig. 5. Result of the joint inversion. An ensemble of dispersion curves of the fundamental mode of Love waves (a), fundamental (b) and first higher (c) mode of Rayleigh waves, and ellipticities of fundamental mode of Rayleigh waves (bold curve – the chunk used in the inversion, dotted curve – f-k ellipticity curve, dashed curve – mean wavelet based ellipticity curve). Observed curves used in the inversion are in black, the color distinguishes the misfit value. An ensemble of inverted velocity profiles for longitudinal waves (e) and shear waves (f). First 10 m are enlarged in the inset.

The inversion of 1D velocity profiles was performed using the Dinver software that implements the modified Neighborhood Algorithm (Wathelet, 2008). Model was parametrized by 20 layers of fixed thickness and density of 2100 kg/m<sup>3</sup> was used for the final inversion. It was possible to perform joint inversion of the dispersion curves (fundamental modes of both Love and Rayleigh waves and first higher mode of Rayleigh waves) and ellipticity (fundamental Rayleigh) with a reasonable result (Fig. 5). Retrieved shear wave velocity profiles are reliable down to 60 m. Shear wave velocities reach 150 m/s in the uppermost layers. A first strong velocity contrast is present at 6 m depth (shear wave velocity increases by factor of two). Another strong velocity contrast is present at the depth of 40 - 50 m (shear wave velocity increases by factor of three). The resulting profiles were compared with the borehole log (Buser, personal communication). The shallow (6 m) interface is too deep to be linked with the water table. It delimitates probably different layers of unconsolidated sands and silts. The configuration of alternating silty, sandy and gravelly layers can be found in most places in the river plain of the Rhone in the Visp area. The second velocity contrast agrees well with the transition from sands and gravels to compacted moraine. The bedrock which is present at 100 m depth according to borehole is not resolved by the array measurement at all.

Summarizing the results for the other arrays (not presented here, see Burjanek *et al.*, 2010b), shear wave velocities reach 150-200 m/s in the shallowest layers (<20 m). These layers are variable in thickness and velocity throughout the city, and we measured the variability in composition of these surface sediments. Below these low-velocity layers the shear wave velocity increases gradually to 300-500 m/s reaching the strong interface at the depth of 40-60 m (shear wave velocity increases here up to factor of three). This interface was identified by all arrays in the area, and linked to the transition from sands and gravels to compacted moraine. The resolution of the shear wave velocities is limited below this interface.

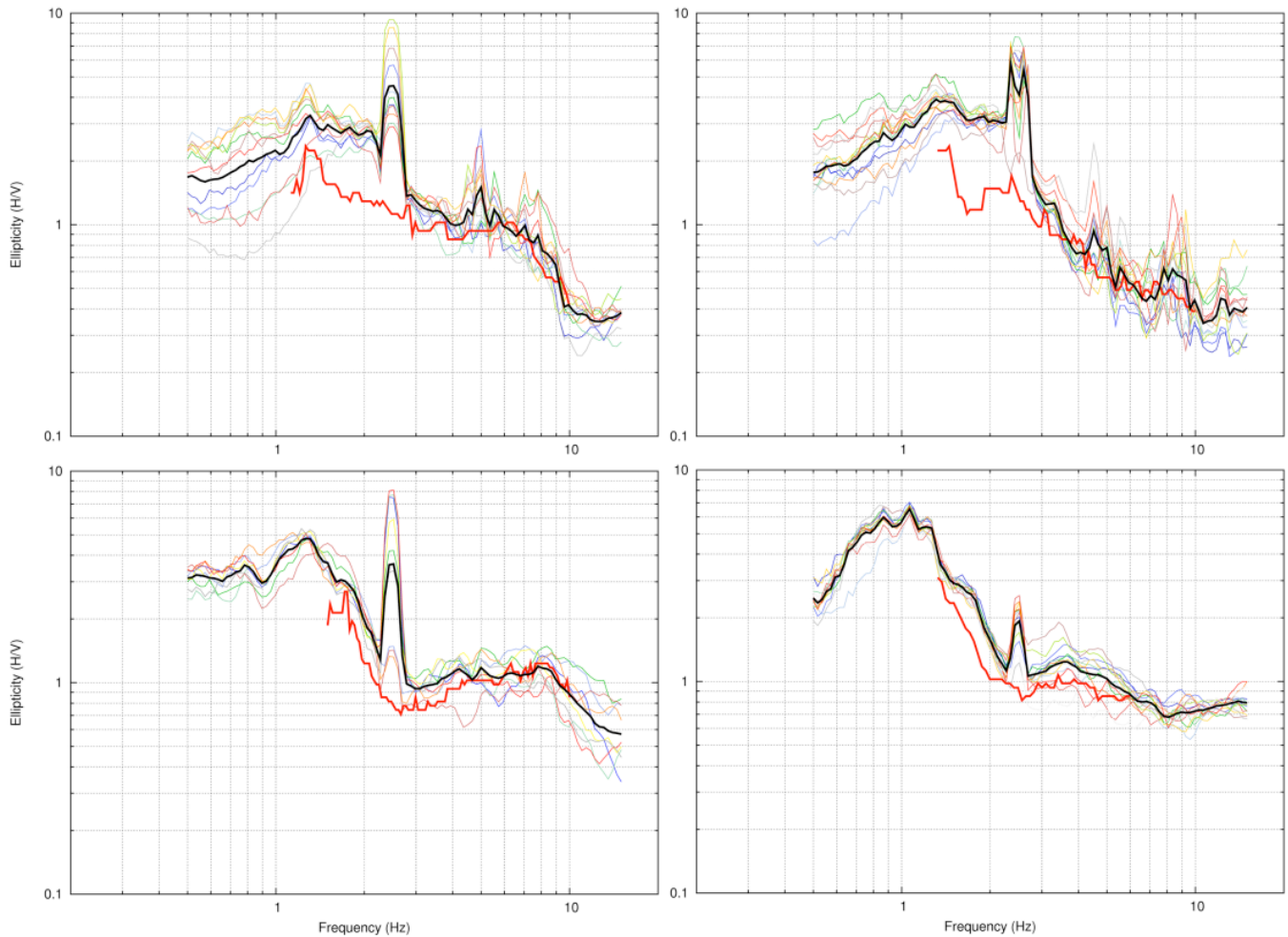


Fig. 6. Comparison between Rayleigh wave ellipticity curves obtained by TFA (thin solid curves – single stations of the array, black bold curve - mean curve across array) and *f-k* method (bold red curve) for four different arrays in Visp area. A peak at 2.5 Hz has an industrial origin.

Finally, we present a comparison between Rayleigh wave ellipticity curve obtained by the new wavelet-based (TFA) and f-k methods (Fig. 6). Ellipticity obtained by the f-k method is always below ellipticity obtained by the wavelet-based method close to the fundamental frequency. The discrepancy is strong for some of the arrays (Fig. 6, top row). The ellipticity estimated by the f-k should not be (in theory) influenced by the body waves or Love waves, and thus should be preferable. Nevertheless, joint inversions of the dispersion and ellipticity curves always preferred the curves retrieved by the wavelet-based method. An explanation might be the contamination of the radial component by the transversal component in the f-k analysis. This explanation is plausible in case of the Brigerbad array (Fig. 4), where the dispersion curve picked for the radial component jumps to Love dispersion curve (below 3 Hz), and the ellipticity obtained by the f-k method does not follow below 3 Hz the curve obtained by the wavelet method.

### Single station measurements

All single-station measurements were processed by different H/V methods (Stamm *et al.*, 2009), and the fundamental frequency was identified for each site. The fundamental frequency was used for the inversion of the bedrock depth in the next section.

### DEVELOPMENT OF A 3D MODEL

First, we test the reliability of the retrieved shear wave velocity profiles by comparing the observed site-to-reference spectral ratios (SRSR) with the synthetic S-wave transfer functions. Two of the temporary stations (VISP1, VISP2) were located close to the array measurements (Fig. 2). The result of the comparison is presented in Fig. 7. The array measurements were not able to resolve deep bedrock, which had to be introduced artificially (shear wave velocity of 2500 m/s; VISP1 – 250 m depth; VISP2 – 150 m depth) to fit the fundamental peak of the observed spectral ratios. The peak of the synthetic transfer functions close to 2.5 Hz suggests, that the industrial noise localized around 2.5 Hz might be amplified by the local structure.

Second, we followed a two step procedure described by Poggi *et al.* (2011) to estimate the basin geometry. In first step, a reference shear wave velocity profile was estimated by averaging the result from the array survey, as the scatter of the retrieved velocity profiles was not large. Two strong interfaces are present in the reference profile. The first interface is present around 50 m depth, and does not change systematically across the Visp area (as discussed in the section about the array measurements). On the other hand, the depth of the second velocity contrast – bedrock interface – is variable (100 m near borehole, 250 m close to VISP2; see Fig. 2). In the second step, we estimate the bedrock depth by fitting the fundamental frequencies estimated previously at 150 different sites with the single station noise measurements. The estimated bedrock depth is presented in Fig. 8. The presence of the two strong interfaces in the shear wave velocity profile makes the bedrock depth estimation difficult. Relatively fast consolidated sediments in the lower layer make the fundamental frequency extremely sensitive to the bedrock depth. In other words, a small error in the fundamental frequency results in the great error in the bedrock depth.

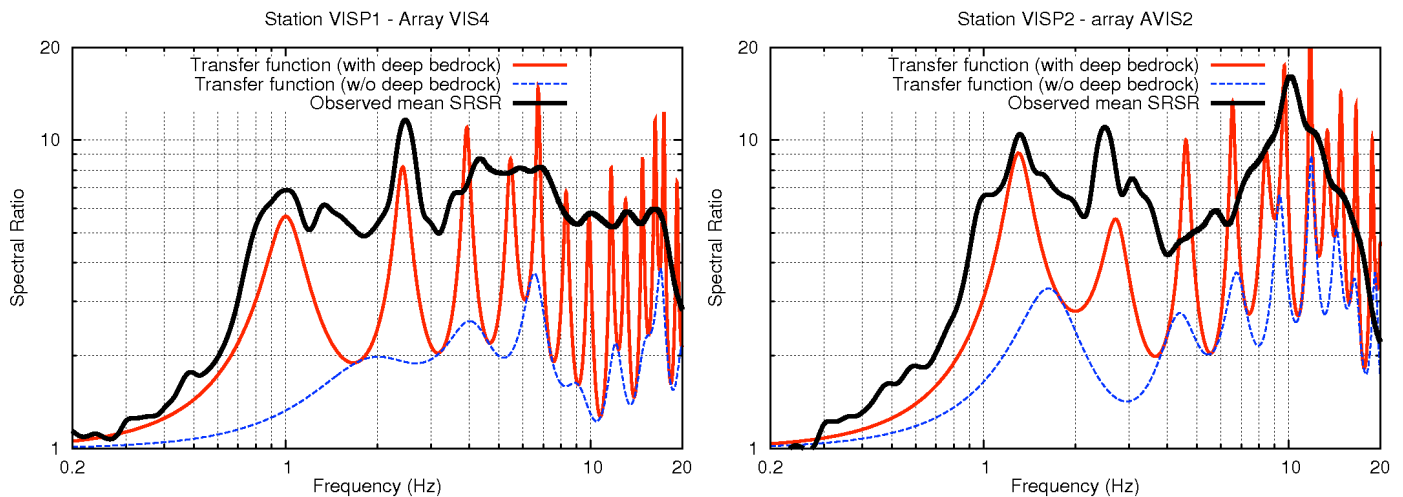


Fig. 7. Comparison between the observed site-to-reference spectral ratios (thick black) and synthetic 1D S-wave transfer functions. Synthetic transfer functions were calculated for two profiles: 1) for the best profile retrieved by array measurement (dashed blue); 2) for the best profile retrieved by array measurement adding deep bedrock (red).

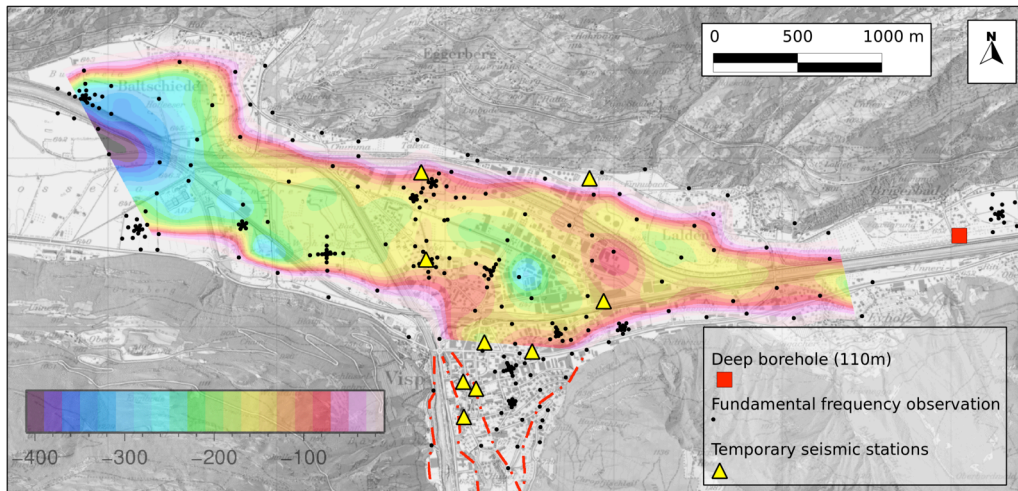


Fig. 8. Color contour plot in the background represents the inverted bedrock depth in the basin. Red dash-dot lines mark the area outside the basin where different sediment types are present.

## CONCLUSIONS

The 3D velocity model of the Visp area is still in the development. The influence of the local soil stratigraphy on amplification and non-linear dynamic behavior (including pore pressure build up and strain-softening) will be further studied with the planned borehole instrumentation (see Fig. 2). We would like to emphasize the application of the three-component f-k method in this study. In general, most of the ambient vibration array measurements are nowadays performed with the three-component seismic sensors, but the horizontal components are usually excluded from the analysis. However, Love wave dispersion curves present a unique constraint on the shear wave velocity profile. Moreover, inconsistencies of the Love and Rayleigh dispersion curves can indicate and address fundamental problems (e.g., anisotropy of the structure; mode mismatching, etc.).

Two techniques to evaluate the Rayleigh ellipticity function have been tested, a single station method and an array method. The two approaches provide comparable results. Ellipticity information obtained in this way can be used as an additional constraint to invert for the velocity structure. Joint inversion of dispersion curves, ellipticity curves and fundamental frequencies enhances the resolution of classical array techniques on deep structures, especially on the depth of the bedrock. This is particularly suitable in densely populated areas, where more sophisticated techniques (e.g., reflection seismics) are generally difficult or even impossible.

Although it is efficient to acquire and analyze ambient vibration data, earthquake recordings still present a unique constraint. Even weak motion data can be useful, e.g., constraining the seismic velocity of the bedrock.

## ACKNOWLEDGEMENTS

Our thanks goes to Marcos Buser, who provided the borehole log. We acknowledge EVWR AG, Lonza AG, Mr. Gurber, Mrs. Salzgeber, Mr. Schaller, Mr. Zuber, and Mr. Zurbriggen for leaving their properties (or properties under their administration) available for the measurement purposes. This research is funded in part by the Competence Center for Environment and Sustainability (CCES) of the ETH Domain, and by the Swiss National Science Foundation. Some figures in this article were made using Generic Mapping Tools (GMT) 4 by Wessel and Smith (1998).

## REFERENCES

- Borcherdt, R.D. [1970], "Effects of local geology on ground motion near San Francisco Bay", *Bull. seism. Soc. Am.*, Vol. 60, pp. 29–61.
- Burjanek, J., G. Gassner-Stamm, and D. Fäh [2010a], "Installation of semi-permanent seismic array and data analysis, COGEAR deliverable 3a.1.1.1", Swiss Seismological Service, Zürich, Switzerland, Report SED/COGEAR/R/005/20100412.
- Burjanek, J., G. Gassner-Stamm, and D. Fäh [2010b], "Array-measurements in the area of Visp and St. Niklaus, COGEAR deliverable 3.1.2", Swiss Seismological Service, Zürich, Switzerland, Report SED/COGEAR/R/003/20100226.

- Capon, J. [1969], "High resolution frequency wavenumber spectrum analysis", Proc. IEEE, Vol. 57, pp. 1408-1418.
- Fäh, D., G. Stamm, and H.-B. Havenith [2008], "Analysis of three-component ambient vibration array measurements", Geophys. Journal International, Vol. 172, pp. 199–213.
- Fäh, D., M. Wathelet, M. Kristekova, H.-B. Havenith, B. Endrun, G. Stamm, V. Poggi, J. Burjanek, and C. Cornou [2009], "*Using ellipticity information for site characterization*", Technical report, NERIES JRA4 Task B2.
- Fäh, D., D. Giardini, P. Kästli, N. Deichmann, M. Gisler, G. Schwarz-Zanetti, S. Alvarez-Rubio, S. Sellami, B. Edwards, B. Allmann, F. Bethmann, J. Wössner, G. Gassner-Stamm, S. Fritsche, and D. Eberhard [2011], "*ECOS-09 Earthquake Catalogue of Switzerland Release 2011. Report and Database. Public catalogue, 17.4.2011.*" Swiss Seismological Service ETH Zürich, Switzerland, Report SED/RISK/R/001/20110417.
- Fritsche, S., D. Fäh, M. Gisler, and D. Giardini [2006], "Reconstructing the Damage Field of the 1855 Earthquake in Switzerland: historical investigations on a well-documented event", Geophys. J. Int., Vol. 166, pp. 719-731.
- Konno, K., and T. Ohmachi [1998], "Ground-Motion Characteristics Estimated from Spectral Ratio between Horizontal and Vertical Components of Microtremor", Bull. Seism. Soc. Am., Vol. 88, pp. 228–241.
- Poggi, V. and D. Fäh [2009]. "Estimating Rayleigh wave particle motion from three-component array analysis of ambient vibrations", Geophys. J. Int., Vol. 180, pp. 251-267.
- Poggi, V., D. Fäh, J. Burjanek, and D. Giardini [2011] "The use of Rayleigh wave ellipticity for site-specific hazard assessment and microzonation. Application to the city of Lucerne, Switzerland", submitted to Geophys. J. Int.
- Stamm, G., D. Fäh, V. Poggi, and I. Löw [2009], "*H/V - measurements in the area of Visp and St. Niklaus, COGEAR deliverable 3.2*", Swiss Seismological Service, Zürich, Switzerland, Report SED/COGEAR/R/001/20090301.
- Wathelet M. [2008], "An improved neighborhood algorithm: parameter conditions and dynamic scaling", Geophys. Res. Lett., Vol. 35, L09301.
- Wathelet, M., D. Jongmans, M. Ohrnberger, and S. Bonnefoy-Claudet [2008], "Array performances for ambient vibrations on a shallow structure and consequences over Vs inversion", J. Seismol., Vol. 12, pp. 1–19.
- Wessel, P., and W. H. F. Smith [1998], "New, improved version of the Generic Mapping Tools released", EOS Trans. AGU, Vol. 79, pp. 579.